

Measurement of the absolute optical properties and cerebral blood volume of the adult human head with hybrid differential and spatially resolved spectroscopy

Terence S Leung¹, Ilias Tachtsidis¹, Martin Smith², David T Delpy¹
and Clare E Elwell¹

¹ Department of Medical Physics & Bioengineering, University College London, Gower Street, London WC1E 6BT, UK

² Department of Neuroanaesthesia & Neurocritical Care, The National Hospital for Neurology & Neurosurgery, London, UK

Received 16 August 2005, in final form 4 December 2005

Published 19 January 2006

Online at stacks.iop.org/PMB/51/703

Abstract

A hybrid differential and spatially resolved spectroscopy (SRS) technique has been developed to measure *absolute* absorption coefficient (μ_a), reduced scattering coefficient (μ'_s) and cerebral blood volume (CBV) in the adult human head. A spectrometer with both differential and SRS capabilities has been used to carry out measurements in 12 subjects. Two versions of the calculation have been considered using the hybrid technique, with one considering water as a chromophore as well as oxy- and deoxy-haemoglobin, and one ignoring water. The CBV has also been measured using a previously described technique based on changing the arterial saturation (SaO₂) measured separately by a pulse oximeter, resulting in mean \pm SD CBV^a (intra-individual coefficient of variation) = 2.22 ± 1.06 ml/100 g (29.9%). (The superscript on CBV indicates the different calculation basis.) Using the hybrid technique with water ignored, CBV⁰ = 3.18 ± 0.73 ml/100 g (10.0%), $\mu_a^0(813 \text{ nm}) = 0.010 \pm 0.003 \text{ mm}^{-1}$ and $\mu'_s^0(813 \text{ nm}) = 1.19 \pm 0.55 \text{ mm}^{-1}$ (data quoted at 813 nm). With water considered, CBV^w = 3.05 ± 0.77 ml/100 g (10.5%), $\mu_a^w(813 \text{ nm}) = 0.010 \pm 0.003 \text{ mm}^{-1}$ and $\mu'_s^w(813 \text{ nm}) = 1.28 \pm 0.56 \text{ mm}^{-1}$. The mean biases between CBV⁰/CBV^w, CBV⁰/CBV^a and CBV^w/CBV^a are 0.14 ± 0.09 , 0.79 ± 1.22 and 0.65 ± 1.24 ml/100 g. The mean biases between $\mu_a^0(813 \text{ nm})/\mu_a^w(813 \text{ nm})$ and $\mu'_s^0(813 \text{ nm})/\mu'_s^w(813 \text{ nm})$ are $(5.9 \pm 10.0) \times 10^{-4} \text{ mm}^{-1}$ and $-0.084 \pm 0.266 \text{ mm}^{-1}$, respectively. The method we describe extends the functionality of the current SRS instrumentation.

(Some figures in this article are in colour only in the electronic version)

1. Introduction

It has been demonstrated that absolute optical properties such as the absorption (μ_a) and reduced scattering coefficients (μ'_s) of human tissues including the head, calf, arm, skin and muscle can be measured using near-infrared (NIR) phase, time or spatially resolved spectroscopy (SRS) systems (Farrell *et al* 1992, Duncan *et al* 1995, Matcher *et al* 1997, Gratton *et al* 1997, Doornbos *et al* 1999). While a continuous-wave system using differential spectroscopy (DS) and a single source-detector spacing can only measure changes of μ_a , i.e. $\Delta\mu_a$, the absolute μ_a cannot be easily measured because of the unknown scattering and geometry dependent losses that occur in the complex tissue geometry in which measurements are made (Delpy and Cope 1997). Subsequently, changes in oxy- and deoxy-haemoglobin concentrations can only be calculated as changes from arbitrary baseline values, i.e. $[\Delta\text{HbO}_2]$ and $[\Delta\text{HHb}]$. It has been shown that a SRS-based technique can be used to calculate a scaled absolute μ_a , i.e. $\mu'_s\mu_a$ where μ'_s is considered as a time-invariant scaling factor (Matcher *et al* 1995, Suzuki *et al* 1999). The NIRO-300 (Hamamatsu Photonics KK) is a commercial spectrometer with both DS and SRS capabilities originally designed to measure changes in haemoglobin concentrations using the measured $\Delta\mu_a$ and a tissue oxygenation index (TOI) using the scaled absolute μ_a . The TOI has been used as a measure to monitor average cerebral oxygenation in various research areas such as obstructive sleep apnoea (Valipour *et al* 2002), liver transplant (Panzer *et al* 2005) and premature infants (Naulaers *et al* 2002). This paper suggests a way to use the NIRO-300 as a platform to estimate absolute μ_a and μ'_s in the human forehead by combining both $\Delta\mu_a$ (calculated from the DS data) and $\mu'_s\mu_a$ (calculated from the SRS data) measurements. Since both DS and SRS data have been used, this technique is referred to as a hybrid DS and SRS technique. The absolute total haemoglobin concentration, $[\text{HbT}]$, and hence cerebral blood volume (CBV) can also be calculated in the process. The hybrid technique discussed here requires the underlying μ_a to vary within a physiologically limited range while μ'_s remains relatively unchanged. Such alterations in μ_a can be achieved by a variety of physiological manoeuvres but in the example reported here are induced by brief hypoxic swings where the fraction of inspired oxygen (FiO_2) is lowered within a small range. During a brief hypoxic episode, arterial oxygen saturation (SaO_2) drops and $[\Delta\text{HbO}_2]$ decreases while $[\Delta\text{HHb}]$ increases; this physiological phenomenon causes a variation in μ_a . Studies have been conducted on 12 adult subjects in which the FiO_2 has been altered. Another aim of this study was to use and to compare two versions of the hybrid DS–SRS technique (where one version takes into account the background water absorption and the other does not) during controlled changes in FiO_2 to estimate absolute μ_a and μ'_s and hence calculate CBV. Finally, we have compared the estimates of CBV made using the hybrid technique with those using a previous technique based on the SaO_2 as measured by a pulse oximeter (Wyatt *et al* 1990, Elwell *et al* 1994, Gupta *et al* 1997, Wolf *et al* 2002) in terms of bias and coefficient of variation.

2. Methodology

2.1. Experiment and instrumentation

Twelve healthy volunteers of mean \pm SD age 32 ± 4 years participated in the studies in which three consecutive graded arterial hypoxaemias were carried out. The study protocol was approved by the local ethics committee and all subjects gave informed consent for participation. A commercial NIR monitor (NIRO-300, Hamamatsu Photonics KK) with both DS and SRS capabilities was used to measure attenuation parameters, including $\Delta A(\lambda)$ at four

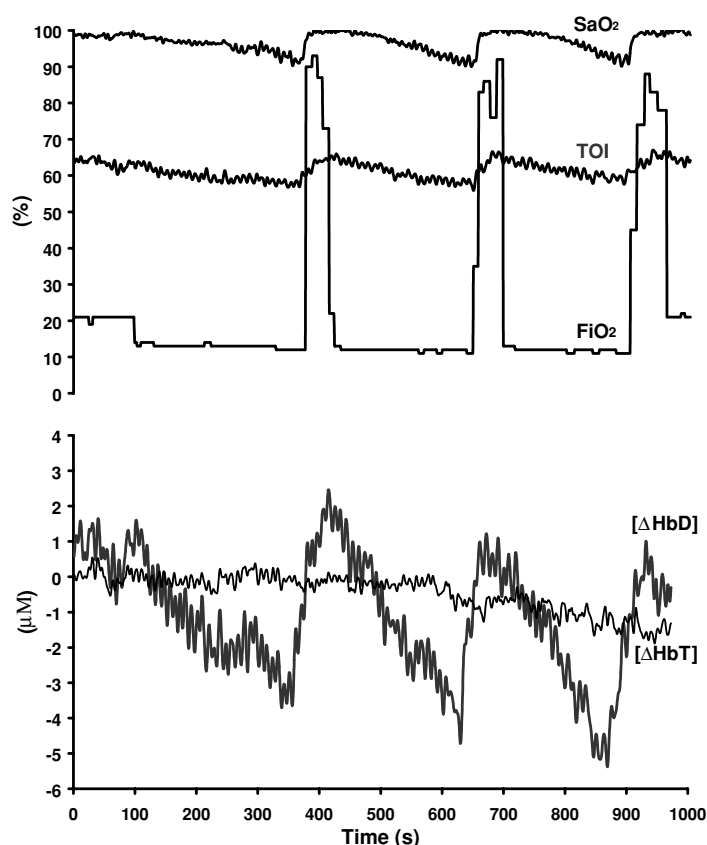


Figure 1. Representative data collected from one volunteer during the three hypoxic episodes.

wavelengths (775, 813, 853 and 910 nm) and $\partial A(\lambda)/\partial \rho$ at three wavelengths (775, 813 and 853 nm), at a sampling rate of 6 Hz. The optodes were placed on the forehead (taking care to avoid the midline sinuses) and were shielded from ambient light by using an elastic bandage and a black cloth. The studies took place in a darkened room. An optode spacing of 4 cm was used. A modified anaesthetics trolley supplied a controlled mixture of nitrogen and oxygen to the subject via a face mask. Arterial saturation was monitored from the ear with a pulse oximeter (Novametrix 500) modified to measure in a beat-to-beat mode. FiO_2 was monitored continuously with a multi-parameter patient monitor (Merlin, Hewlett Packard).

All measurements were made with the volunteers sitting comfortably in an armchair. The subject initially breathed normal air for 3–5 min. The FiO_2 in the circuit was then gradually reduced to 11–15% by mixing air and nitrogen, until a baseline SaO_2 of 90% was achieved. At that point, the subject was given 100% O_2 for five consecutive breaths followed by a return to breathing air. This sequence was repeated for a total of three times for each subject. Figure 1 shows an example of data collected during the experiment. Three hypoxic episodes can be seen with SaO_2 never reaching below 90%. The de-saturation of SaO_2 to 90% is not expected to cause a significant change in cerebral blood flow or oxygen consumption which may affect the validity of the proposed method. A significant rise in cerebral blood flow only occurs when SaO_2 falls below $\sim 75\%$ (Wyatt *et al* 1990, Johannssen and Siesjo 1975, Kogure *et al* 1970). Previous animal and human studies have also shown that slight arterial

hypoxaemia causes no change in global cerebral oxygen consumption (Johannssen and Siesjo 1975, Siesjo 1978).

2.2. Estimation of absorption and reduced scattering coefficients

Based on the modified Beer–Lambert law, the difference between μ_a at two time points, i.e. $\Delta\mu_a$, can be calculated from a measurement of the difference of attenuation at those time points (ΔA):

$$\Delta\mu_a^{\text{DS}} = \frac{\Delta\mathbf{A} \times \ln 10}{\rho \times \text{DPF}} = \varepsilon\Delta\mathbf{C} \quad (\text{mm}^{-1}), \quad (1)$$

where ρ is the optode spacing, DPF is the differential pathlength factor, $\Delta\mathbf{A}$ and $\Delta\mathbf{C}$ are column vectors containing attenuation changes and concentration changes, respectively, and ε is a matrix consisting of the specific absorption coefficients of chromophores at specified wavelengths. The superscript ‘DS’ signifies the association with differential spectroscopy. When ΔA is measured with the log base of 10, the scaling factor $\ln 10$ needs to be introduced to convert equation (1) to the log base of e with which μ_a is defined in the diffusion equation. With μ_a^{DS} measured at two or more wavelengths, preferably with at least one on each side of the isobestic point at 800 nm, $[\Delta\text{HbO}_2]$ and $[\Delta\text{HHb}]$ can be calculated by the least-square fit (Cope 1991). Four wavelengths at 775, 813, 853 and 910 nm have been used here.

Based on the semi-infinite half-space geometry, the solution of the diffusion equation for light transport in tissue in a continuous-wave system can be differentiated with respect to the optode spacing ρ , resulting in an expression for μ_a^{SRS} scaled by μ'_s (Matcher *et al* 1995):

$$\mu'_s\mu_a^{\text{SRS}} = \frac{1}{3} \left(\ln 10 \frac{\partial A}{\partial \rho} - \frac{2}{\rho} \right)^2 \quad (\text{mm}^{-2}), \quad (2)$$

where $\partial A/\partial \rho$ is the attenuation slope measured with multiple detectors and has a log base of 10. To emphasize the significance of the wavelength dependence of μ_a and μ'_s , these values are expressed as functions of λ , i.e. $\mu_a(\lambda)$ and $\mu'_s(\lambda)$ in this section. While the wavelength dependence of $\mu_a(\lambda)$ is a function of all the chromophores’ concentrations in the field of view, the wavelength dependence of $\mu'_s(\lambda)$ in tissues has been found to remain relatively linear. One widely used form of wavelength dependence of $\mu'_s(\lambda)$ is formulated as $\mu'_s(\lambda) = a\lambda^{-b}$, where constants a and b have been estimated experimentally in breast tissue and pig blood (Cerussi *et al* 2001, Durduran *et al* 2002, Srinivasan *et al* 2005). Matcher *et al* measured the wavelength dependence of $\mu'_s(\lambda)$ in human heads and used a different formulation $\mu'_s(\lambda) = k(a\lambda + b)$, where $a = -6.5 \times 10^{-4} \text{ mm}^{-1} \text{ nm}^{-1}$, $b = 1.45 \text{ mm}^{-1}$ and k can be considered as a constant in the NIR region (Matcher *et al* 1997). It should be noted that both formulations result in a $\mu'_s(\lambda)$ which decreases mainly linearly with increasing wavelength in the NIR range. In this paper, we use the latter formulation which is based on measurements on the human head. The linear behaviour of $\mu'_s(\lambda)$ simplifies its estimation at other wavelengths because once $\mu'_s(\lambda^*)$ has been estimated at one wavelength (i.e. λ^*) its values at other wavelengths (i.e. λ) can be approximated by

$$\mu'_s(\lambda) = \frac{a\lambda + b}{a\lambda^* + b} \mu'_s(\lambda^*) = q(\lambda)\mu'_s(\lambda^*), \quad (3)$$

where $q(\lambda^*) = 1$. Equation (2) can now be rewritten as

$$\mu'_s(\lambda^*)\mu_a^{\text{SRS}}(\lambda) = \frac{1}{3q(\lambda)} \left(\ln 10 \frac{\partial A(\lambda)}{\partial \rho} - \frac{2}{\rho} \right)^2. \quad (4)$$

Equation (4) is similar to an equation in Suzuki *et al* (1999) except here $\mu_a^{\text{SRS}}(\lambda)$ is scaled by $\mu'_s(\lambda^*)$ rather than k . In the following, we consider three wavelengths, say $\lambda_1, \lambda_2, \lambda_3$ and we choose $\lambda^* = \lambda_1$. The scaled chromophore concentrations can now be estimated by a least-square fit:

$$\mu'_s(\lambda_1)\mathbf{C} = [\varepsilon_{i,j}]^{-1} \begin{bmatrix} \mu'_s(\lambda_1)\mu_a^{\text{SRS}}(\lambda_1) \\ \mu'_s(\lambda_1)\mu_a^{\text{SRS}}(\lambda_2) \\ \mu'_s(\lambda_1)\mu_a^{\text{SRS}}(\lambda_3) \end{bmatrix}, \quad (5)$$

where $j = \lambda_1, \lambda_2, \lambda_3$ and \mathbf{C} is a column vector containing absolute chromophore concentrations. Equation (5) shows that using $\mu'_s(\lambda)\mu_a^{\text{SRS}}(\lambda)$ calculated from the attenuation slope ($\partial A(\lambda)/\partial \rho$), the product of $\mu'_s(\lambda)$ and the absolute concentrations can be obtained. We will use the superscripts '0' (water ignored) and 'w' (water considered) to distinguish how the chromophore concentrations are calculated. We consider \mathbf{C} and $\varepsilon_{i,j}$ in two cases. In the first case, $\mathbf{C} = [\text{HHb}^0 \text{HbO}_2^0]^T$ (where T is the transpose) and $i = \text{HHb}^0, \text{HbO}_2^0$. The first case corresponds to the approach adopted in Suzuki *et al* (1999), who converted the scaled $\mu_a^{\text{SRS}}(\lambda)$ into scaled $[\text{HHb}]$ and $[\text{HbO}_2]$ using a least-square fit having ignored the absorption caused by water and other background absorbers such as melanin and lipids. In the second case, $\mathbf{C} = [\text{HHb}^w \text{HbO}_2^w \text{H}_2\text{O}^w]^T$ and $i = \text{HHb}^w, \text{HbO}_2^w, \text{H}_2\text{O}^w$ which corresponds to the conversion of scaled $\mu_a^{\text{SRS}}(\lambda)$ into three major (scaled) chromophores in the NIR region, i.e. $[\text{HHb}]$, $[\text{HbO}_2]$ and water (Cope 1991, Sevick *et al* 1991). The inclusion of water in the conventional least-square fit, i.e. pseudo inverse, often leads to erroneous negative values of absolute water concentrations. A least-square algorithm with non-negativity constraints has been used here to perform the conversion (Lawson and Hanson 1974). The values of $[\text{HHb}^w]$ and $[\text{HbO}_2^w]$ are expected to be smaller than those of $[\text{HHb}^0]$ and $[\text{HbO}_2^0]$ because the same amount of attenuation now accounts for one more chromophore, i.e. water.

Suppose FiO_2 has now been changed and SaO_2 drops slightly well inside the cerebral autoregulation levels without causing any changes in CBV, cerebral blood flow or oxygen consumption. This leads to a change in $[\Delta\text{HbO}_2]$ and $[\Delta\text{HHb}]$, and thus μ_a while μ'_s remains essentially constant. In such a case, one can often find that $[\Delta\text{HbO}_2]$ and $[\Delta\text{HHb}]$ follow the same time course but in opposite directions. One can therefore approximate $[\Delta\text{HbO}_2] \approx -[\Delta\text{HHb}]$ and thus $[\Delta\text{HbD}] = [\Delta\text{HbO}_2] - [\Delta\text{HHb}] \approx 2[\Delta\text{HbO}_2]$.

The relationship between $[\Delta\text{HbD}]$ calculated from equation (1) and $\mu'_s(\lambda_1) \cdot [\text{HbD}]$ calculated from equation (5) can be expressed as

$$\mu'_s(\lambda_1) \cdot [\text{HbD}] = \mu'_s(\lambda_1)([\Delta\text{HbD}] + [\text{HbD}_{\text{base}}]), \quad (6)$$

where $[\text{HbD}_{\text{base}}]$ is the baseline value which has been deducted from subsequent values of $[\text{HbD}]$. By plotting measurements of $[\Delta\text{HbD}]$ (x -axis) against those of $\mu'_s(\lambda_1) \cdot [\text{HbD}]$ (y -axis), one can theoretically get a straight line in an ideal noise-free case with the y -intercept = $\mu'_s(\lambda_1) \cdot [\text{HbD}_{\text{base}}]$ and the gradient of the straight line = $\mu'_s(\lambda_1)$. In reality, data points are scattered around the theoretical straight line due to noise. Since we expect errors in both $[\Delta\text{HbD}]$ and $\mu'_s(\lambda_1) \cdot [\text{HbD}]$, the gradient or $\mu'_s(\lambda_1)$ in this case is found by using the total least squares method (Van Huffel and Vanderwalle 1991) to fit a straight line between $[\Delta\text{HbD}]$ and $\mu'_s(\lambda_1) \cdot [\text{HbD}]$ as shown in figure 2 (to be discussed further in section 2.4). Unlike linear regression which only minimizes the vertical distances between data points and the regressed straight line, total least squares minimizes the perpendicular distances which accounts for errors in both $[\Delta\text{HbD}]$ in the x -axis and $\mu'_s(\lambda_1) \cdot [\text{HbD}]$ in the y -axis. As mentioned earlier, $\mu'_s(\lambda)$ at other wavelengths can be estimated from $\mu'_s(\lambda_1)$ using equation (3). Subsequently, $\mu_a^{\text{SRS}}(\lambda)$ can be found simply by dividing $\mu'_s(\lambda_1)\mu_a^{\text{SRS}}(\lambda)$ by $\mu'_s(\lambda_1)$.

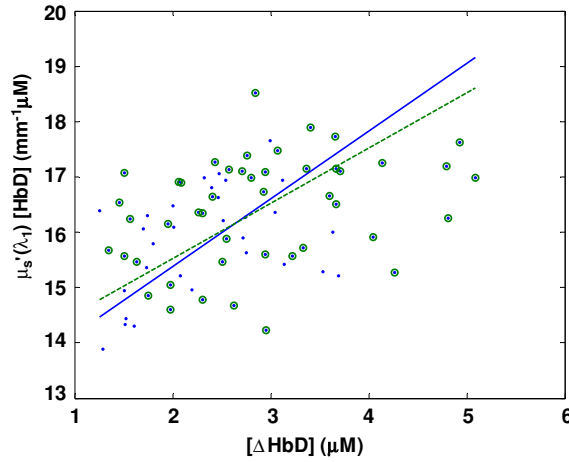


Figure 2. Finding $\mu'_s(\lambda_1)$ by exploiting the linear relationship between $[\Delta\text{HbD}]$ and $\mu'_s(\lambda_1) \cdot [\text{HbD}]$. Solid dots correspond to all data points during a hypoxic episode while circles correspond to data points with $[\Delta\text{HbT}]$ varying within $\pm 0.5 \mu\text{M}$ about the mean. The solid straight line provides the gradient of all data points (solid dots) = $\mu'_s(\lambda_1) = 1.22 \text{ mm}^{-1}$. The dotted straight line provides the gradient of selected data points (circle) = $\mu'_s(\lambda_1) = 1.00 \text{ mm}^{-1}$.

It is also worth mentioning that an alternative approach of estimating $\mu'_s(\lambda_1)$ from $\Delta\mu_a^{\text{DS}}(\lambda_1)$ of equation (1) and $\mu'_s(\lambda_1)\mu_a^{\text{SRS}}(\lambda)$ of equation (4) is to fit a straight line between these two measurements and the gradient is then $\mu'_s(\lambda_1)$ (Leung *et al* 2003). Using this approach, $\mu'_s(\lambda_1)$ is estimated by the use of two attenuation measurements, namely $\Delta A(\lambda_1)$ and $\partial A(\lambda_1)/\partial\rho$ at the same wavelength. However, the results obtained from this alternative approach are more susceptible to noise compared to that described here. This is because instead of two raw measurements, the technique introduced here makes use of seven attenuation measurements, namely $\Delta A(\lambda)$ at four wavelengths and $\partial A(\lambda)/\partial\rho$ at three wavelengths, which tends to reduce the effects of noise.

2.3. Estimation of cerebral blood volume with tissue oxygenation index

One possibility of estimating $[\text{HbT}]$ once $\mu'_s(\lambda_1)$ has become available is to divide $\mu'_s(\lambda_1) \cdot [\text{HbT}] = \mu'_s(\lambda_1)([\text{HbO}_2] + [\text{HHb}])$ by $\mu'_s(\lambda_1)$. This approach creates one value of $[\text{HbT}]$ for every value of $\mu'_s(\lambda_1) \cdot [\text{HbT}]$ and the result is directly affected by the accuracy of $\mu'_s(\lambda_1)$. Instead, we have used the following approach based on the TOI to avoid using $\mu'_s(\lambda_1)$ in the estimation of $[\text{HbT}]$. The TOI is defined as

$$\text{TOI} = \frac{\mu'_s(\lambda_1)[\text{HbO}_2]}{\mu'_s(\lambda_1)([\text{HbO}_2] + [\text{HHb}])} \times 100\% = \frac{[\text{HbO}_2]}{[\text{HbO}_2] + [\text{HHb}]} \times 100\% \quad (7)$$

and is calculated from the attenuation measurements $\partial A(\lambda)/\partial\rho$ via equations (4) and (5), and with $\mu'_s(\lambda_1)$ cancelling out. As mentioned in section 2.2, there are two ways of calculating $\mu'_s(\lambda_1) \cdot [\text{HbO}_2]$ and $\mu'_s(\lambda_1) \cdot [\text{HHb}]$ in the conversion from scaled $\mu_a(\lambda)$ to scaled concentrations, one which includes the absorption due to water and the other without. Subsequently, we consider two versions of TOI signified by superscripts, i.e. TOI^0 (water ignored) and TOI^w (water considered).

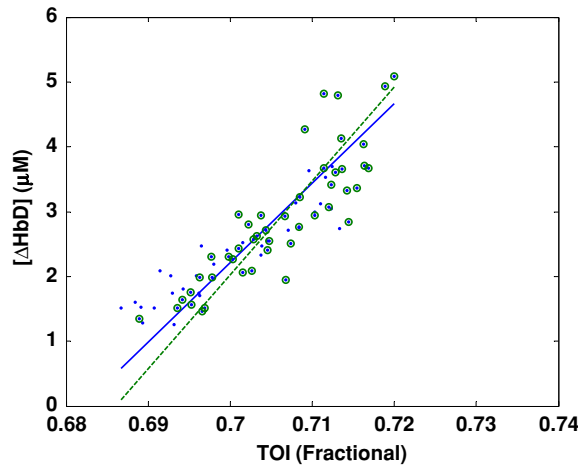


Figure 3. Finding [HbT] by exploiting the linear relationship between TOI^0 and $[\Delta\text{HbD}]$. Solid dots correspond to all data points during a hypoxic episode while circles correspond to data points with $[\Delta\text{HbT}]$ varying within $\pm 0.5 \mu\text{M}$ about the mean. The solid straight line is the gradient of all data points (solid dots) $\equiv 2[\text{HbT}]$ (i.e. $[\text{HbT}] = 61.3 \mu\text{M}$). The dotted straight line is the gradient of selected data points (circle) $\equiv 2[\text{HbT}]$ (i.e. $[\text{HbT}] = 72.5 \mu\text{M}$). The correlation coefficient of the selected data points is 0.87.

In a situation whereby FiO_2 is carefully adjusted while keeping the CBV, CBF and oxygen consumption relatively constant, $[\Delta\text{HbO}_2]$ and ΔTOI will both change in proportion and their relationship can be expressed as

$$[\text{HbT}] = \frac{[\Delta\text{HbO}_2]}{\Delta\text{TOI}} = \frac{[\Delta\text{HbD}]}{2\Delta\text{TOI}}, \quad (8)$$

where TOI is either TOI^0 or TOI^w and we again assume $[\Delta\text{HbO}_2] \approx -[\Delta\text{HbD}]$. As shown in figure 3, which will be discussed further in section 2.4, values of $[\Delta\text{HbD}]$ and TOI^0 are plotted against each other during a hypoxic episode. A straight line can be found by performing total least squares on the data points and its gradient is [HbT] as suggested by equation (8). This approach is very similar to an earlier technique based on arterial saturation (SaO_2) measured from a pulse oximeter (Wyatt *et al* 1990, Elwell *et al* 1994, Gupta *et al* 1997, Wolf *et al* 2002), except TOI instead of SaO_2 has been used here. The [HbT] and hence CBV estimated using SaO_2 has also been calculated for comparison in the following analysis.

2.4. Data selection

In sections 2.2 and 2.3, we propose the use of total least squares to estimate $\mu'_s(\lambda_1)$ from equation (6) and [HbT] from equation (8), via the gradients of regressed lines. Strictly speaking, the linear nature of this approach makes it valid only when the underlying parameter, i.e. either $\mu'_s(\lambda_1)$ or [HbT], stays constant during a hypoxic manoeuvre. In reality, we can tolerate moderate variations of the underlying $\mu'_s(\lambda_1)$ or [HbT]. The value of $\mu'_s(\lambda_1)$ is normally quite stable over time unless there is a large change of the number of scatterers in the tissues, which could be caused by a large change in the number of red blood cells or blood volume. Therefore, the stability of [HbT] can in a way reflect that of $\mu'_s(\lambda_1)$ and we will focus on the variation of [HbT] in the following discussion. Figure 4(a) shows the variation of [HbT] as indicated by $[\Delta\text{HbT}]$ calculated from the modified Beer–Lambert law of equation (1) during a hypoxic episode. It can be seen that $[\Delta\text{HbT}]$ can vary by as much as $\pm 2 \mu\text{M}$. If all the

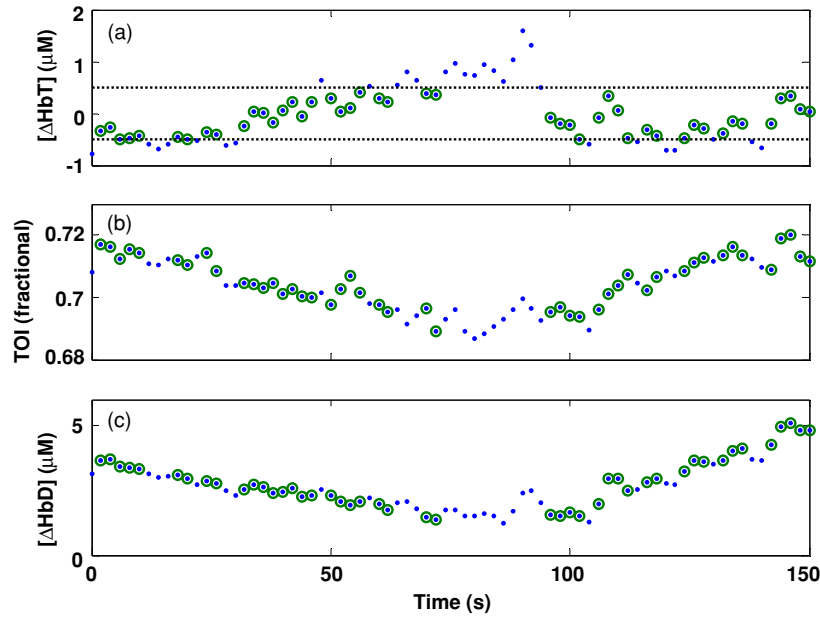


Figure 4. Data points corresponding to (a) $[\Delta\text{HbT}]$, (b) TOI and (c) $[\Delta\text{HbD}]$. Data points are selected only when their corresponding $[\Delta\text{HbT}]$ vary within $\pm 0.5 \mu\text{M}$ about the mean. Solid dots are all the data points in a hypoxic episode while circles correspond to selected data points.

corresponding data points are to be included in the estimation of $[\text{HbT}]$, the accuracy of the result will be affected because equation (8) is not always valid for all the data points. The strategy adopted here is to only include data points whose corresponding $[\Delta\text{HbT}]$ vary within certain defined limits of the mean level of $[\Delta\text{HbT}]$, which have been set to $\pm 0.5 \mu\text{M}$ (determined from experience) in this work for adult subjects. In other words, we only select data points for analysis when equation (8) is deemed applicable. Figures 4(b) and (c) show the corresponding selected data points for TOI and $[\Delta\text{HbD}]$, respectively. In figure 2, a total least squares has been performed on $\mu'_s(\lambda_1) \cdot [\text{HbD}]$ and $[\Delta\text{HbD}]$ to estimate $\mu'_s(\lambda_1)$. In this example, $\mu'_s(\lambda_1) = 1.22 \text{ mm}^{-1}$ without any selection of data points and $\mu'_s(\lambda_1) = 1.00 \text{ mm}^{-1}$ using only the selected data points. In figure 3, a total least squares has been performed on $[\Delta\text{HbD}]$ and TOI^0 to estimate $[\text{HbT}]$. In this case, $[\text{HbT}] = 61.3 \mu\text{M}$ without any selection of data points and $[\text{HbT}] = 72.5 \mu\text{M}$ using only the selected data points.

One way to check the applicability of equation (8) is to consider the correlation coefficient between $[\Delta\text{HbD}]$ and TOI. The correlation coefficient of the selected data points is as high as 0.87 in the example given in figure 3 indicating a good reliability of the results. From experience, a correlation coefficient smaller than 0.8 is taken to indicate a potential violation of assumptions behind equation (8) and the corresponding data points are considered unsuitable for the estimation of $[\text{HbT}]$ and $\mu'_s(\lambda_1)$.

2.5. Conversion from the absolute haemoglobin concentration to the cerebral blood volume

Blood consists of both haemoglobins and plasma but $[\text{HbT}]$ only accounts for haemoglobin concentration in *tissues*. To convert $[\text{HbT}]$ into CBV, we need to divide $[\text{HbT}]$ by the average haemoglobin concentration in the *cerebral blood* but this cannot easily be measured non-

invasively. Instead, the haemoglobin concentration in blood is measured from the peripheral circulation and the average cerebral haemoglobin concentration estimated using the cerebral large-to-small vessel haematocrit ratio (CLVHR). This ratio accounts for the reduced red cell content of blood in the cerebral vessels compared to that in the large venous vessels (due to the Fahraeus effect) from which the blood sample has been taken (Wyatt *et al* 1990). The following formula has been used for the conversion:

$$CBV = \frac{[HbT] \times MW_{Hb} \times 10^{-5}}{d_t \times Hb_t \times CLVHR} \quad (\text{ml}/100 \text{ g}), \quad (9)$$

where $MW_{Hb} = 64\,500 \text{ g}$ is the molecular weight of haemoglobin, $d_t = 1.05 \text{ g ml}^{-1}$ is the cerebral tissue density (Nelson *et al* 1971), $Hb_t \text{ (g dl}^{-1}\text{)}$ is the haemoglobin concentration obtained from a venous sample and $CLVHR = 0.69$ (Lammertsma *et al* 1984). Equation (9) has been used in previous studies to convert $[HbT]$ into CBV (Wyatt *et al* 1990, Elwell *et al* 1994, Gupta *et al* 1997, Wolf *et al* 2002, Leung *et al* 2004). A variation of the formula has also been employed in a CBV study using indocyanine green as the tracer (Hopton *et al* 1999).

2.6. Data analysis

In the following analysis, the differential pathlength factor (DPF) was determined by an equation accounting for the age dependence: $DPF(780 \text{ nm}) = 5.13 + 0.07AGE^{0.81}$, where $AGE = 32$ (mean age of the subjects). In this study, all subjects were in the same age group and one differential pathlength factor value of 6.3 (calculated using the mean age) was used for all analyses. This equation is based on a study of 283 subjects whose age ranges from 1 day to 50 years (Duncan *et al* 1996). In order to remove cardiac-related and spontaneous oscillations (Elwell *et al* 1999, Obrig *et al* 2000), the $[\Delta HbO_2]$, $[\Delta HHb]$, TOI (TOI^0 and TOI^w) and SaO_2 signals were low-pass filtered with a fifth-order Butterworth filter at a cut-off frequency of 0.2 Hz. Using the techniques introduced in sections 2.2 and 2.4, two sets of $\mu'_s(\lambda)$ at 775, 813 and 853 nm were calculated using $[\Delta HbD^0]$ and $[\Delta HbD^w]$, respectively, for each hypoxic episode. In the data selection, only those data points corresponding to a $[\Delta HbT]$ of less than $\pm 0.5 \mu\text{M}$ were included in the analysis. Once $\mu'_s(\lambda)$ has been estimated, $\mu_a(\lambda)$ at 775, 813 and 853 nm can also be estimated at 6 Hz (the sampling rate). Averaged $\mu_a(\lambda)$ was then calculated over 20 s of a normoxic period when subjects were breathing room air. Using the approaches discussed in sections 2.3–2.5, three sets of $[HbT]$ and CBV were calculated for each hypoxic episode, respectively, which used (a) TOI^0 , (b) TOI^w and (c) SaO_2 . For the first two TOI -based methods, both the de-saturation and the re-saturation periods were used. Since SaO_2 was measured at the ear lobes and $[\Delta HbD]$ was measured at the forehead, there was a time delay between these signals. This delay was manually corrected for in the data before further analysis was performed. In the SaO_2 method, the linear regression method (instead of the total least squares method) has been used to calculate $[HbT] = [\Delta HbD]/(2\Delta SaO_2)$ following the practice in previous studies (Wyatt *et al* 1990, Elwell *et al* 1994, Gupta *et al* 1997).

3. Results

3.1. Cerebral blood volume

The correlation coefficient between $[\Delta HbD]$ and TOI/SaO_2 during a hypoxic episode was used to assess whether there was sufficient linear relationship between these two parameters and hence whether the resulting CBV measurement was valid. A total of 36 hypoxic episodes from 12 subjects (three hypoxaemias from each subject) were recorded in this study. Using

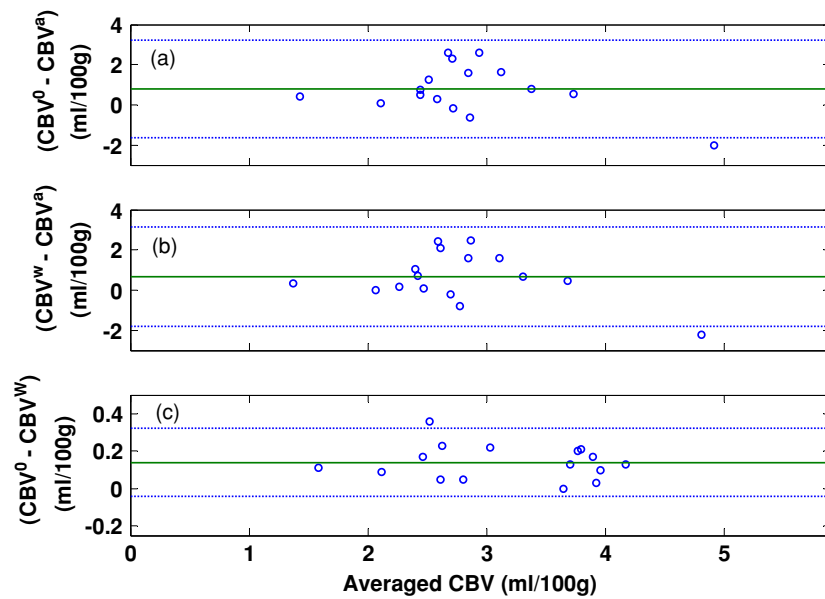


Figure 5. Bland–Altman plots: CBV difference versus averaged CBV. The solid line corresponds to the mean difference and dotted lines mean \pm 2SD. (a) CBV^0 and CBV^a ; bias = 0.79 ± 1.22 ml/100 g; (b) CBV^w and CBV^a ; bias = 0.65 ± 1.24 ml/100 g; (c) CBV^0 and CBV^w ; bias = 0.14 ± 0.09 ml/100 g.

a threshold of 0.8 for the correlation coefficient, 27 measurements from 10 subjects were considered valid for the calculation of both CBV^0 (using TOI^0 with water ignored) and CBV^w (using TOI^w with water considered), and 21 measurements from 9 subjects were valid for the calculation of CBV^a (using SaO_2). The excluded hypoxic episodes were considered to be affected by movement artefacts or by changes of the other monitored physiological parameters. In one subject, none of the data achieved the required threshold, and so the whole data set was excluded from the analysis. The mean \pm SD CBV using the three approaches were $CBV^0 = 3.18 \pm 0.73$ ml/100 g, $CBV^w = 3.05 \pm 0.77$ ml/100 g and $CBV^a = 2.22 \pm 1.06$ ml/100 g.

In order to assess the repeatability of each analysis method, CBV results from subjects having three valid hypoxic episodes were used to calculate the intra-individual coefficients of variation. These were 10.0% for CBV^0 ($n = 9$), 10.5% for CBV^w ($n = 8$) and 29.9% CBV^a ($n = 4$).

The degrees of agreement using the three analysis methods were analysed using a Bland–Altman analysis (Bland and Altman 1986). Out of a total of 36 hypoxic episodes, 20 from eight subjects were considered valid for CBV estimations using all three analysis methods. The rest of the hypoxic measurements were deemed invalid in one or more analysis methods. The biases (mean difference \pm SD) calculated from the Bland–Altman plots in figure 5 are summarized in table 1.

3.2. Absorption and reduced scattering coefficients

The means and standard deviations of $\mu'_s(\lambda)$ and $\mu_a(\lambda)$ calculated using the $[\Delta HbD^0]$ (with water ignored) and $[\Delta HbD^w]$ (with water considered) are summarized in table 2. As discussed in section 2.2, $\mu'_s(\lambda)$ at one wavelength was estimated from a hypoxic measurement and $\mu'_s(\lambda)$ at the other two wavelengths were simply calculated by scaling using equation (3). Therefore,

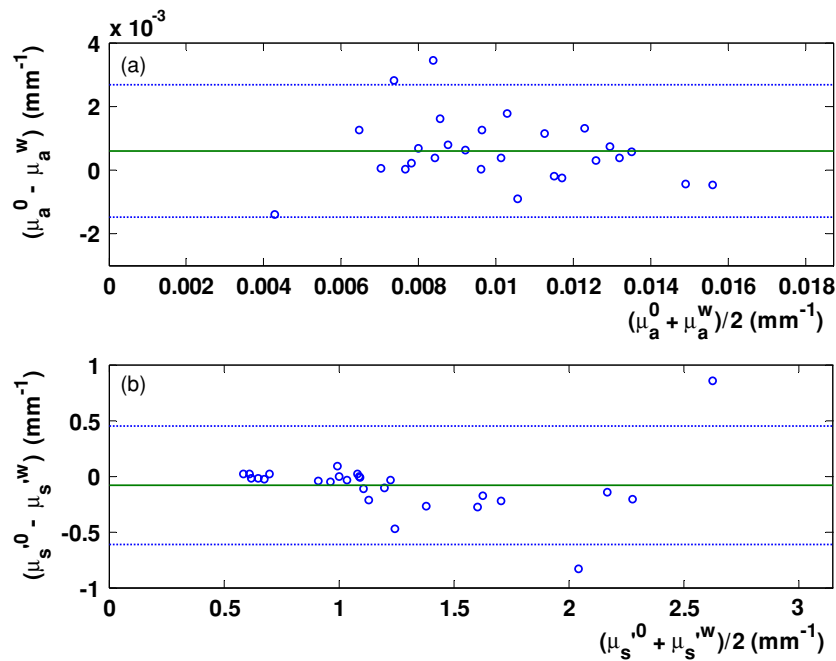


Figure 6. Bland–Altman plots: the solid line corresponds to the mean difference and dotted lines mean \pm 2SD. (a) μ_a^0 and μ_a^w at 813 nm; bias = $(5.9 \pm 10.0) \times 10^{-4} \text{ mm}^{-1}$; (b) μ_s^0 and μ_s^w at 813 nm; bias = $-0.084 \pm 0.266 \text{ mm}^{-1}$.

Table 1. Bias (mean difference and standard deviation) of CBV between two analysis methods as calculated by the Bland–Altman analysis plotted in figure 5.

Bias between the two methods	Mean difference \pm standard deviation (ml/100 g)
CBV ⁰ and CBV ^w	0.14 \pm 0.09
CBV ⁰ and CBV ^a	0.79 \pm 1.22
CBV ^w and CBV ^a	0.65 \pm 1.24

Table 2. Mean and standard deviation of μ'_s and μ_a at $\lambda = 775, 813$ and 853 nm estimated using the hybrid technique with and without taking water into consideration ($n = 27$).

	Mean \pm standard deviation (mm^{-1})					
	$\mu'_s(775 \text{ nm})$	$\mu'_s(813 \text{ nm})$	$\mu'_s(853 \text{ nm})$	$\mu_a(775 \text{ nm})$	$\mu_a(813 \text{ nm})$	$\mu_a(853 \text{ nm})$
Using $[\Delta\text{HbD}^0]$ without considering water	1.22 \pm 0.57	1.19 \pm 0.55	1.16 \pm 0.54	0.010 \pm 0.003	0.010 \pm 0.003	0.013 \pm 0.003
Using $[\Delta\text{HbD}^w]$ with water considered	1.31 \pm 0.58	1.28 \pm 0.56	1.24 \pm 0.54	0.009 \pm 0.003	0.010 \pm 0.003	0.012 \pm 0.003

the coefficient of variation of $\mu'_s(\lambda)$ calculated from three hypoxic measurements was the same for all the three wavelengths. As for $\mu_a(\lambda)$, the coefficient of variation was also the same for the three wavelengths. This was because firstly the same resting period had been used for the calculation of an averaged $\mu_a(\lambda)$ in the three hypoxic measurements and secondly the

Table 3. Bias (mean difference and standard deviation) of μ'_s/μ_a between two analysis methods, i.e. with (μ_s^w/μ_a^w) and without (μ_s^0/μ_a^0) water considered at $\lambda = 775, 813$ and 853 nm, as calculated by the Bland–Altman analysis plotted in figure 6.

Bias between the two methods	Mean difference \pm standard deviation (mm^{-1})		
	$\lambda = 775$ nm	$\lambda = 813$ nm	$\lambda = 853$ nm
$\mu_s^0(\lambda)$ and $\mu_s^w(\lambda)$	-0.086 ± 0.273	-0.084 ± 0.266	-0.081 ± 0.258
$\mu_a^0(\lambda)$ and $\mu_a^w(\lambda)$	$(5.4 \pm 9.6) \times 10^{-4}$	$(5.9 \pm 10.0) \times 10^{-4}$	$(7.4 \pm 13.0) \times 10^{-4}$

estimation of $\mu_a(\lambda)$ involved the use of $\mu'_s(\lambda)$ which as already discussed was different for the three wavelengths by only a scaling factor. The intra-individual coefficient of variation of $\mu_s^0(\lambda)$ (with water ignored) was 8.8% ($n = 9$) and that of $\mu_s^w(\lambda)$ (with water considered) was 9.3% ($n = 8$). The intra-individual coefficient of variation of $\mu_a^0(\lambda)$ was 8.9% ($n = 9$) and that of $\mu_a^w(\lambda)$ was 9.3% ($n = 8$).

A Bland–Altman analysis was carried out for 27 hypoxic measurements. The biases (mean difference \pm SD) between $\mu_s^0(\lambda)$ and $\mu_s^w(\lambda)$ and between $\mu_a^0(\lambda)$ and $\mu_a^w(\lambda)$ at three wavelengths are summarized in table 3. The Bland–Altman plot for $\mu_s^0(813$ nm) and $\mu_s^w(813$ nm) and that for $\mu_a^0(813$ nm) and $\mu_a^w(813$ nm) are given in figure 6. The Bland–Altman plots for μ_s^0/μ_s^w and μ_a^0/μ_a^w at the other two wavelengths, i.e. 775 nm and 853 nm, are similar to those in figure 6 and are not shown here. No particular structures are evident in the errors shown in these Bland–Altman plots, suggesting the absence of systematic errors.

4. Discussion and conclusions

We have developed a hybrid DS and SRS technique to calculate μ'_s , μ_a and CBV in the adult head. This work extends the functionality of a type of NIRS systems based on the SRS principle (e.g. NIRO-300, NIRO-200 and NIRO-100, Hamamatsu Photonics KK). Two versions of the same calculation have been discussed, namely one considering water (resulting in μ_s^w , μ_a^w and CBV^w) and one without (resulting in μ_s^0 , μ_a^0 and CBV^0). For CBV, the results from the hybrid technique have been compared with those from an existing technique based on SaO_2 . The mean CBVs calculated from the three methods (i.e. $\text{CBV}^0 = 3.18 \pm 0.73$ ml/100 g, $\text{CBV}^w = 3.05 \pm 0.77$ ml/100 g and $\text{CBV}^a = 2.22 \pm 1.06$ ml/100 g) are comparable to the published results in one study of 2.85 ± 0.97 ml/100 g for adults (Elwell *et al* 1994). To find the gradient between ΔSaO_2 and $[\Delta\text{HbD}]$, previous CBV studies have performed linear regression which only accounts for errors in the y-axis only, i.e. $[\Delta\text{HbD}]$ (Wyatt *et al* 1990, Elwell *et al* 1994). In one CBV study, a scheme was proposed to minimize errors in both ΔSaO_2 and $[\Delta\text{HbD}]$ which is based on a function of averaging the gradients of two regressed lines, i.e. regressing ΔSaO_2 on $[\Delta\text{HbD}]$ and regressing $[\Delta\text{HbD}]$ on ΔSaO_2 (Wolf *et al* 1997). In the current study, a more straightforward technique known as total least squares (Van Huffel and Vanderwalle 1991), which minimize the perpendicular distances between data points and the regressed line, has been used. The gradients and hence CBV (i.e. CBV^0 and CBV^w) estimated using total least squares tend to be higher than those obtained using linear regression (i.e. CBV^a), as evident from our results.

Other NIR-based studies of CBV in the literature have reported a range of different results. While one study based on SaO_2 reported a higher value of CBV of 5.38 ml/100 g (Gupta *et al* 1997), another study using ICG as the tracer reported a lower value of 1.1 ± 0.39 ml/100 g (Hopton *et al* 1999). The discrepancies could be due to the use of different instruments,

differential pathlength factors and tracers. In a SPECT study, a CBV of 4.81 ± 0.37 ml/100 g has been reported for regional brain tissues (Sakai *et al* 1985).

As an imaging technique, the SPECT result contains data only from the brain tissue whereas NIR systems probe all the tissues between the optodes including scalp, skull and brain, resulting in an averaged tissue blood volume, which may be lower than that of the brain alone. Out of 36 hypoxic episodes, the hybrid technique has resulted in a higher number of valid CBV measurements of 27, compared to the SaO₂-based technique which had 21. The robustness of the hybrid technique is further demonstrated by its intra-individual coefficients of variation of 10.0% (water ignored) and 10.5% (water considered), compared to the SaO₂-based technique value of 29.9%. The lack of robustness of the SaO₂-based technique is not a surprise considering that the technique involves two separate instruments, namely a pulse oximeter and a tissue spectrometer, and also requiring the manual synchronization of their signals. In comparison, the hybrid technique is more direct and simple and only one spectrometer with DS and SRS capabilities is needed.

It is theoretically more 'correct' to consider water in the calculation. However, the mean difference and especially the SD between CBV⁰ and CBV^w are small (0.14 ± 0.09 ml/100 g), showing that CBV⁰ can be used in place of CBV^w with only moderate differences (CBV⁰ is higher than CBV^w by approximately 4.6%). The hybrid technique including water requires an iterative least-square algorithm with non-negativity constraints which increases the intra-individual coefficient of variation slightly because an additional concentration (water) is also estimated. The algorithm is also more computationally expensive than the simple arithmetic operations required by the hybrid technique with the water ignored. The SDs of differences between CBV⁰ and CBV^a (1.22 ml/100 g) and between CBV^w and CBV^a (1.24 ml/100 g) are both large showing that the degree of agreement between the hybrid techniques and the SaO₂-based technique is limited.

The mean μ'_s and μ_a at the three wavelengths (775, 813 and 853 nm) with water considered are very close to those with water ignored. The mean $\mu'_s(813 \text{ nm}) = 1.19 \pm 0.55 \text{ mm}^{-1}$ is comparable to the previously published result of $\mu'_s(800 \text{ nm}) = 0.94 \pm 0.07 \text{ mm}^{-1}$ using a time-resolved system (Matcher *et al* 1997), while the mean $\mu_a(813 \text{ nm}) = 0.010 \pm 0.003 \text{ mm}^{-1}$ is lower than that obtained in the same time-resolved study $\mu_a(800 \text{ nm}) = 0.016 \pm 0.001 \text{ mm}^{-1}$. The SDs of both $\mu'_s(813 \text{ nm})$ and $\mu_a(813 \text{ nm})$ are comparatively larger than those obtained using a time-resolved system. The intra-individual coefficients of variation of μ'_s^w and μ_a^w are slightly higher than those of μ'_s^0 and μ_a^0 again due to the use of the iterative least-square algorithm with non-negativity constraints when water is considered. The mean difference of $-0.084 \pm 0.266 \text{ mm}^{-1}$ at 813 nm shows that μ'_s^0 is smaller than μ'_s^w by approximately 7%, while μ_a^0 is slightly larger than μ_a^w by approximately 6% with a mean difference of $(5.9 \pm 10.0) \times 10^{-4} \text{ mm}^{-1}$ at 813 nm.

One has to be careful when it comes to the interpretation of μ'_s , μ_a and CBV estimated here. First, as mentioned earlier, in the calculation of μ'_s , μ_a and CBV, a pre-defined constant known as the differential pathlength factor is required. Depending on the location of the measurement site and the age of the subject, the differential pathlength factor can vary from 5.13 in infants to 6.26 in adults (Duncan *et al* 1996). It has also been reported that the differential pathlength factor has a standard deviation of approximately 15% among the same group of subjects which also affects the accuracy of the estimates of μ'_s , μ_a and CBV. By adding a pathlength measuring capability to the existing SRS system (whether through the use of phase or time based measurement), the differential pathlength factor could be measured for individual subjects and hence improve the accuracy of the estimated μ'_s , μ_a and CBV. Second, the technique assumes the tissues to be homogenous rather than layered and inhomogeneous as is found in reality. The estimated μ'_s , μ_a and blood volume are therefore

averaged values for all tissues in the field of view including the skin, skull, cerebrospinal fluid and brain, rather than just for a specific layer such as the brain. Third, in the conversion from [HbT] to CBV, the scaling factor known as the cerebral to large vessel haematocrit ratio is used to compensate for the reduced red cell content of blood in cerebral vessels compared to that in the large vessels due to the Fahraeus effect. The exact value of this scaling factor is still a subject of controversy with values ranging from the 0.69 used here (Lammertsma *et al* 1984) to 0.75 (Sakai *et al* 1985).

The continuous-wave system used in this study employs simple and economical optoelectronic devices compared to its frequency/time domain counterparts which require frequency modulation or photon counting. The frequency/time domain systems can however measure the differential pathlength directly and do not rely on a pre-set differential pathlength factor, resulting in more accurate results.

Acknowledgments

The authors would like to thank Dr C Oliver, Dr H Jones and all the volunteers who participated in this study. This work was funded by the Wellcome Trust (GR 061558) and also supported by Hamamatsu Photonics KK.

References

- Bland J M and Altman D G 1986 Statistical methods for assessing agreement between two methods of clinical measurements *Lancet* **8** 307–10
- Cerussi A E, Berger A J, Bevilacqua F, Shah N, Jakubowski D, Butler J, Holcombe R F and Tromberg B J 2001 Sources of absorption and scattering contrast for near-infrared optical mammography *Acad. Radiol.* **8** 211–8
- Cope M 1991 The application of near-infrared spectroscopy to non-invasive monitoring of cerebral oxygenation in the newborn infant *PhD Thesis* University College London
- Delpy D T and Cope M 1997 Quantification in tissue near-infrared spectroscopy *Philos. Trans. R. Soc. Lond. B: Biol. Sci.* **352** 649–59
- Doornbos R M P, Lang R, Aalders M C, Cross F W and Sterenborg H J C M 1999 The determination of *in vivo* human tissue optical properties and absolute chromophore concentrations using spatially resolved steady-state diffuse reflectance spectroscopy *Phys. Med. Biol.* **44** 967–81
- Duncan A, Meek J H, Clemence M, Elwell C E, Fallon P, Tyszczuk L, Cope M and Delpy D T 1996 Measurement of cranial optical path length as a function of age using phase resolved near infrared spectroscopy *Pediatr. Res.* **39** 889–94
- Duncan A, Meek J H, Clemence M, Elwell C E, Tyszczuk L, Cope M and Delpy D T 1995 Optical pathlength measurements on adult head, calf and forearm and the head of the newborn-infant using phase-resolved optical spectroscopy *Phys. Med. Biol.* **40** 295–304
- Durduran T, Choe R, Culver J P, Zubkov L, Holboke M J, Giammarco J, Chance B and Yodh A G 2002 Bulk optical properties of healthy female breast tissue *Phys. Med. Biol.* **47** 2847–61
- Elwell C E, Cope M, Edwards A D, Wyatt J S, Delpy D T and Reynolds E O 1994 Quantification of adult cerebral hemodynamics by near-infrared spectroscopy *J. Appl. Physiol.* **77** 2753–60
- Elwell C E, Springett R, Hillman E and Delpy D T 1999 Oscillations in cerebral haemodynamics—implications for functional activation studies *Adv. Exp. Med. Biol.* **471** 57–65
- Farrell T J, Patterson M S and Wilson B C 1992 A diffusion theory model of spatially resolved, steady state diffuse reflectance for the noninvasive determination of tissue optical properties *in vivo Med. Phys.* **19** 879–88
- Gratton E, Fantini S, Franceschini M A, Gratton G and Fabiani M 1997 Measurements of scattering and absorption changes in muscle and brain *Philos. Trans. R. Soc. Lond. B: Biol. Sci.* **352** 727–35
- Gupta A K, Menon D K, Czosnyka M, Smielewski P, Kirkpatrick P J and Jones J G 1997 Non-invasive measurement of cerebral blood volume in volunteers *Br. J. Anaesth.* **78** 39–43
- Hopton P, Walsh T S and Lee A 1999 Measurement of cerebral blood volume using near-infrared spectroscopy and indocyanine green elimination *J. Appl. Physiol.* **87** 1981–7
- Johannssen H and Siesjo B K 1975 Cerebral blood flow and oxygen consumption in the rat in hypoxic hypoxia *Acta Physiol. Scand.* **93** 515–25

- Kogure K, Scheinberg P, Reinmuth O M, Fujishima M and Busto R 1970 Mechanisms of cerebral vasodilatation in hypoxia *J. Appl. Physiol.* **29** 223–9
- Lammertsma A A, Brooks D J, Beaney R P, Turton D R, Kensett M J, Heather J D, Marshall J and Jones T 1984 *In vivo* measurement of regional cerebral haematocrit using positron emission tomography *J. Cereb. Blood Flow Metab.* **4** 317–22
- Lawson C and Hanson R 1974 *Solving Least Squares Problems* (Englewood Cliffs, NJ: Prentice-Hall)
- Leung T S, Elwell C E, Tachtsidis I, Henty J R and Delpy D T 2003 Measurement of the optical properties of the adult human head with spatially resolved spectroscopy and changes of posture *Adv. Exp. Med. Biol.* **540** 13–8
- Leung T S, Narendra A, Elwell C E, Delpy D T and Costeloe K 2004 A new method for the measurement of cerebral blood volume and total circulating blood volume using near infrared spatially resolved spectroscopy and indocyanine green: application and validation in neonates *Pediatr. Res.* **55** 134–41
- Matcher S J, Cope M and Delpy D T 1997 *In vivo* measurements of the wavelength dependence of tissue-scattering coefficients between 760 and 900 nm measured with time-resolved spectroscopy *Appl. Opt.* **36** 386–96
- Matcher S J, Kirkpatrick P, Nahid K, Cope M and Delpy D T 1995 Absolute quantification methods in tissue near infrared spectroscopy *Proc. SPIE* **2389** 486–95
- Naulaers G, Morren G, Van Huffel S, Casaer P and Devlieger H 2002 Cerebral tissue oxygenation index in very premature infants *Arch. Dis. Child. Fetal Neonatal Ed.* **87** 189–92
- Nelson S R, Mantz M L and Maxwell J A 1971 Use of specific gravity in the measurement of cerebral edema *J. Appl. Physiol.* **30** 268–71
- Obrig H, Neufang M, Wenzel R, Kohl M, Steinbrink J and Villringer A 2000 Spontaneous low frequency oscillations of cerebral haemodynamics and metabolism under rest and visual stimulation in adults *NeuroImage* **12** 623–39
- Panzer P, Cicco G, Memeo R, Catalano G, Greco L, Staffieri F, Lupo L and Memeo V 2005 Predictive value of alterations of brain perfusion during liver transplantation *Transplant. Proc.* **37** 2622–5
- Sakai F, Nakazawa K, Tazaki Y, Ishii K, Hino H, Igarashi H and Kanda T 1985 Regional cerebral blood volume and haematocrit measured in normal human volunteers by single-photon emission computed tomography *J. Cereb. Blood Flow Metab.* **5** 207–13
- Sevick E M, Chance B, Leigh J, Nioka S and Maris M 1991 Quantitation of time- and frequency-resolved optical spectra for the determination of tissue oxygenation *Anal. Biochem.* **195** 330–51
- Siesjo B K 1978 *Brain Energy Metabolism* (New York: Wiley) p 423
- Srinivasan S, Pogue B W, Jiang S, Dehghani H and Paulsen K D 2005 Spectrally constrained chromophore and scattering near-infrared tomography provides quantitative and robust reconstruction *Appl. Opt.* **44** 1858–69
- Suzuki S, Takasaki S, Ozaki T and Kobayashi Y 1999 A tissue oxygenation monitor using NIR spatially resolved spectroscopy *Proc. SPIE* **3597** 582–92
- Valipour A, McGown A D, Makker H, O’Sullivan C and Spiro S G 2002 Some factors affecting cerebral tissue saturation during obstructive sleep apnoea *Eur. Respir. J.* **20** 444–50
- Van Huffel S and Vanderwalle J 1991 *The Total Least Squares Problem: Computational Aspects and Analysis* (Philadelphia, PA: SIAM)
- Wyatt J S, Cope M, Delpy D T, Richardson C E, Edwards A D, Wray S and Reynolds E O 1990 Quantitation of cerebral blood volume in human infants by near-infrared spectroscopy *J. Appl. Physiol.* **68** 1086–91
- Wolf M, Bucher H U, Dietz V, Keel M, von Siebenthal K and Duc G 1997 How to evaluate slow oxygenation changes to estimate absolute cerebral haemoglobin concentration by near infrared spectrophotometry in neonates *Adv. Exp. Med. Biol.* **428** 495–501
- Wolf M, von Siebenthal K, Matthias K, Dietz V, Baenziger O and Bucher H U 2002 Comparison of three methods to measure absolute cerebral hemoglobin concentration in neonates by near infrared spectrophotometry *J. Biomed. Opt.* **7** 221–7